INTERNATIONAL JOURNAL OF ROBUST AND NONLINEAR CONTROL
Int. J. Robust Nonlinear Control 2005; **15**:821–837
Published online in Wiley InterScience (www.interscience.wiley.com). DOI: 10.1002/rnc.1026

A robust control based solution to the sample-profile estimation problem in fast atomic force microscopy

Srinivasa M. Salapaka[1,*,†], Tathagata De[2,‡] and Abu Sebastian[3,§]

[1] *Mechanical and Industrial Engineering, UI Urbana-Champaign, IL 61821, U.S.A.*
[2] *Electrical and Computer Engineering, Iowa State University, Ames, IA 50011, U.S.A.*
[3] *IBM Zurich Research Laboratory, CH-8803 Rüschlikon, Switzerland*

SUMMARY

The atomic force microscope (AFM) is a powerful tool for imaging and manipulating matter at the nanoscale. An optimal control problem is proposed for the control of AFMs which includes the design of a sample-profile estimate signal in addition to the set-point regulation and resolution objectives. A new estimate signal for the sample profile is proposed and it is proved that the transfer function between the profile signal and the estimate signal is unity. The main contribution in comparison to existing designs is that there is no bandwidth limitation on estimation of sample profiles! Experimental results are presented to corroborate these results. Copyright © 2005 John Wiley & Sons, Ltd.

KEY WORDS: estimation; sample profile; robust control; atomic force microscopy; fast scan

1. INTRODUCTION

The atomic force microscope (AFM), since its invention in 1986 [1], continues to have a deep impact in many areas of science and technology. The primary component of an AFM is a micro-cantilever with an ultra sharp tip that has a diameter of a few nanometers. The micro-cantilever has a relatively small spring constant but has high resonant frequency due to the small mass. The small stiffness facilitates detection of the extremely small interactive forces between the tip and the sample whereas the high resonant frequency reduces the effect of various sources of vibration. The AFM is most widely used to obtain the topography of samples with sub-nanometer resolution. Besides topographical imaging, the AFM has enabled probing and manipulation of different physical variables that include magnetic, electrical, biological, and chemical properties in the nanoscale [2–4]. However, its considerable potential still needs to be

*Correspondence to: Srinivasa M. Salapaka, Mechanical and Industrial Engineering, UI Urbana-Champaign, IL 61821, U.S.A.
† E-mail: salapaka@uiuc.edu
‡ E-mail: tatha@iastate.edu
§ E-mail: ase@zurich.ibm.com

Contract/grant sponsor: NSF; contract/grant numbers: ECS 0449310 CAR, CMS 0301516, CMS 0201560

 Accepted 22 July 2005

tapped. There is still a lot of scope for improvement of these devices in achieving high resolution images at higher bandwidth. In this context, the control design forms an important component towards achieving these goals. This has led to a growing interest in atomic force microscopy in the systems and dynamical systems communities. System tools have been used to study steady state behaviour of cantilevers [5, 6], explain rich complex behaviour observed in experiments [7–9], and derive fundamental limitations on this technology [10]. The need for high throughputs in many applications has imposed severe demands on these devices. Several system theoretic methods are being applied to address this need such as increasing the detection bandwidth using observer based control scheme in Reference [11] and increasing the throughput by implementing an array of cantilevers by using analysis and control tools from the area of distributed control theory [12, 13]. Significant research has been done in the area of sample positioning for the AFM [14–18]. Piezo-actuators are widely used for sample positioning. However, piezo-actuation introduces effects such as hysteresis, drift and creep which adversely affect the performance of the device. System tools have been applied to study these effects and compensate for them. The classical PID-design, which is typically employed for control in these devices is inadequate, in many cases, to realize their full potential. Consequently, robust control tools have been proposed and implemented which have shown substantial improvement in *simultaneously* achieving fine resolution, high bandwidth and robustness of these devices.

Compared to the research on sample positioning, the equally important problem of obtaining signals which are accurate measures of the sample topography has received little attention. In this paper, we address this problem especially for fast imaging applications. It forms an important step towards building a robust high precision microscope with ultrafast imaging capability. In a typical imaging operation, the sample positioning controller moves the sample up or down to maintain a set-point deflection for the micro-cantilever while the cantilever scans over the sample surface. The control effort u which is the input to the vertical positioner is typically used as an estimate of the sample topography, which is satisfactory for slow scans but not for fast scans of rough surfaces. In Reference [15] the idea of using a simulation of the positioner dynamics to obtain better estimates of the sample profile is presented. However, this leads to added complexity in the design and is more susceptible to model uncertainties. Sebastian *et al*. [19] present the idea of using better sample-profile estimate signals derived from the controller instead of the control effort u. These signals are considerably better for fast scans but are still bandwidth limited. The main contribution of this paper is that we propose a new estimate signal and prove that it asymptotically tracks the profile perfectly for *all* frequencies, i.e. the transfer function between the estimate signal and the sample profile signal is equal to one! The proposed signal is obtained by exploiting the 'quasi-observer' form of the central $\mathscr{H}_\infty$-controller and the structure of the model for the device. It comes at no extra computational cost over the control design—The $\mathscr{H}_\infty$ controller is designed to obtain set point regulation and high resolution and the proposed profile estimate signal is derived in terms of this controller. This scheme is demonstrated by simulation and experimental results.

An optimal control problem is proposed which includes the objectives of high resolution, set point regulation and low profile estimation error. We show that the proposed signal is a solution to this problem. Moreover, we study its robustness to modelling uncertainties. The paper is organized as follows. In Section 2 the device set up and the optimal problem formulation is presented. In Section 3 the new signal is proposed and its robustness properties are investigated. The experimental results are presented in Section 4.

2. SETUP AND PROBLEM FORMULATION

A schematic of an AFM and its working principle is illustrated in Figure 1. Typically the AFM is used in either of the two modes of operations, dynamic-mode and contact-mode. In the dynamic-mode operation the cantilever is made to oscillate and the changes to the periodic orbit due to tip–sample interactions give a measure of the sample profile. In contact-mode operation the cantilever tip rides on top of the sample and the cantilever deflections due to tip–sample interactions give a measure of the profile. When these deflections are directly used for imaging (the controller in Figure 1 is disabled) as in *constant height operation*, the contact forces can vary which typically result in unreliable and distorted images and sometimes tip–sample damage. Therefore in a typical contact mode operation, the cantilever deflection is regulated at a set-point (i.e. the tip–sample force is kept constant) while scanning the sample. This is achieved by moving the vertical positioner (Z-piezo) to which the cantilever is attached up or down to compensate for the undulations in the sample surface by using a feedback controller. The input to the vertical positioner, i.e. the compensating control signal, is traditionally used as a measure of the sample profile. However, this method of imaging is valid only for low bandwidth imaging applications.

Figure 2 shows a system theoretic model of an AFM. Here G_z represents the vertical positioner, G_c represents the microcantilever, S_D represents the deflection transducer and K is the control transfer function. The cantilever tip encounters the surface topography as a time signal $d(t) = h(x(t), y(t))$ where $h(\cdot, \cdot)$ represents the sample profile and $(x(t), y(t))$ denotes the lateral co-ordinates of the tip sample contact point set by the X–Y scanner. This sample profile signal d is viewed as a 'disturbance' signal which tries to deviate the cantilever deflection signal from its set point deflection (see Figure 2(a)). We simplify this diagram by combining the transfer functions G_z, G_c and S_D as in Figure 2(b). If we assume that G_c is equal to a constant S_C (which is a good approximation since micro-cantilevers have much larger bandwidths than the vertical scanners), then $\tilde{d}$ represents a scaled sample profile.

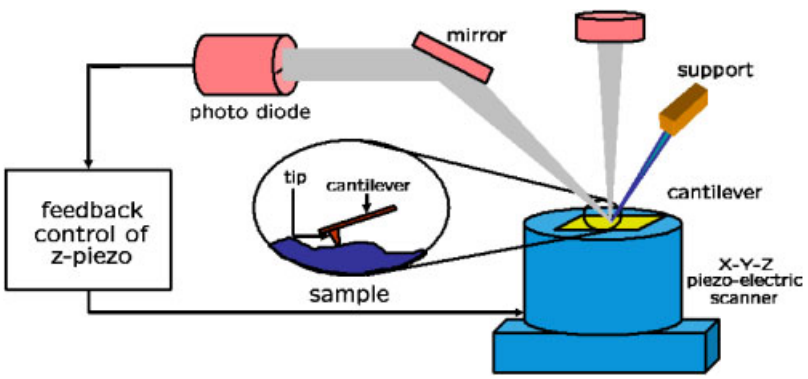

Figure 1. Schematic of an AFM. The primary component is a micro-cantilever. The cantilever deflection is sensed by a laser incident on the back of the cantilever reflecting into a split-photodiode. The sample is positioned using nano-positioners. In contact mode operation, the photodiode output is utilized by a feedback controller to maintain a constant deflection and the control signal gives an estimate of the sample profile.

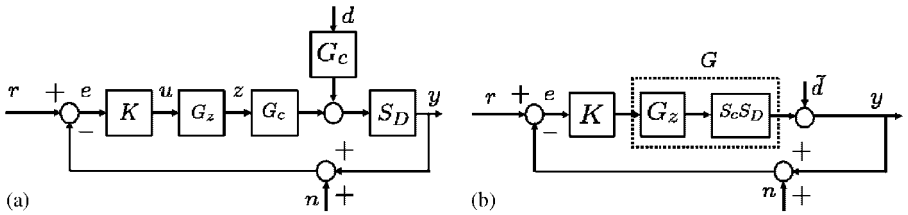

Figure 2. (a) The block diagram modelling of the AFM where $G_c, G_z K, S_{\mathrm{D}}$ are the cantilever, piezo-scanner, controller and the deflection transducer transfer functions, respectively. The signals r, y, e and n are the setpoint, the cantilever deflection, the deflection error and the transducer noise, respectively. The signal d models the sample topography; and (b) G represents a combination of the scanner, lever and the transducer dynamics. The cantilever has high resonant frequency and is assumed to be a constant over the frequency region of interest. Hence $\tilde{d}$ is a scaled version of the sample topography.

The inadequacy of the control signal as an imaging signal at high frequencies is explained by looking at the requirements on control design. It is required that there is good set point regulation to avoid tip-sample damage and to retain the validity of the model. A good set point regulation over a pre-specified bandwidth is achieved by designing K to have high gain over the bandwidth. This is easily seen from the transfer function from set point r to the regulation error e given by the sensitivity function $S = 1/(1 + G(j\omega)K(j\omega))$ which is small when $|K(j\omega)|$ is large.

Moreover, the transfer function from the sample profile $\tilde{d}$ to the control signal u is $K(j\omega)/(1 + K(j\omega)G(j\omega))$ which is $\approx 1/G(j\omega)$ for large K. Typically the positioner transfer function $G(j\omega)$ is approximately a constant at low frequencies and thus the control signal u is a good estimate of the sample profile. However, at high frequencies $G(j\omega)$ is not constant and the dynamics of the positioner has to be dealt with. The control signal is clearly an inaccurate estimate of the sample profile at these frequencies. Also note that the temporal frequency content of $\tilde{d}$ depends on the spatial frequency content of the sample, i.e. how *rough* the sample is, and the scanning rate of the lateral positioners, i.e how *fast* the sample is scanned. In view of new control designs [14, 16–18] for faster lateral positioning it is imperative to obtain better estimates of $\tilde{d}$ especially with high frequency content.

The controller design to use the control effort for imaging is seen in conjunction with other important objectives imposed on it. The principal objectives on control design include achieving set-point regulation over high bandwidths, obtaining images with high resolution and keeping control signal within saturation limits of the piezoelectric scanner. High bandwidths are required to maintain a small deflection error signal which avoid tip-sample damages in fast scanning of *rough* surfaces (having high spatial frequency content) and to keep the validity of the *linear* model while at the same time stringent resolution requirements impose limitations on bandwidths since a wider bandwidth integrates more sensor noise into the system. It needs to be emphasized that the ultimate goal of microscopy is imaging; the resolution and regulation objectives are futile if the imaging objective is not achieved. In this context, we lay down an optimal control problem which captures all these objectives (see Figure 3). In this formulation, the set point regulation, the high resolution and bounded control objectives are captured by the regulated outputs $z_1 = W_S e,\ z_2 = W_T v,\ z_3 = W_u u$ and $z_4 = W_d e_d$ where $W_S,\ W_T$ and W_u are appropriately chosen weighting functions [20]. The main contribution of this paper is addressing the objective of finding a sample profile estimate. This is captured by requiring the

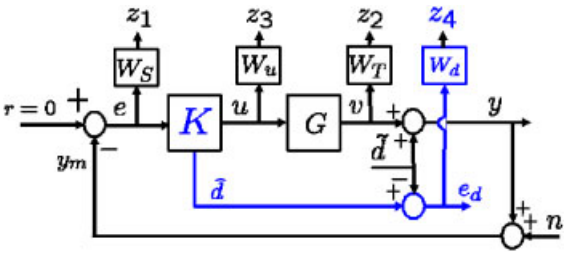

Figure 3. Framework for the optimal control problem. The block $K = [K_1 \;\; K_2]^{\mathrm{T}}$ has two outputs—the control signal u with the objective of achieving robust set point regulation of the deflection signal y and high resolution through roll off of the transfer function from the setpoint r to the piezo response v; and the signal $\hat{d}$ with the objective of giving an accurate estimate of the sample profile $\tilde{d}$. Our design objective is to minimize weighted performance variable z_1 (weighted regulation error), z_2 (weighted noise sensitivity), z_3 (weighted control effort) and z_4 (weighted estimation error).

estimate error $W_d(\hat{d} - \tilde{d})$ to be small. Thus the transfer function P from $[r - n \;\; \tilde{d}]^{\mathrm{T}}$ to z is described by

$$\begin{bmatrix} z_1 \\ z_2 \\ z_3 \\ z_4 \end{bmatrix} = \begin{bmatrix} W_S S & -W_S S \\ W_T T & -W_T T \\ W_u K_1 S & -W_u K_1 S \\ W_d K_2 S & -W_d(1 + K_2 S) \end{bmatrix} \begin{bmatrix} r - n \\ \tilde{d} \end{bmatrix} \tag{1}$$

where $S = 1/(1 + GK_1)$ is the sensitivity and $T = 1 - S$ is the complementary sensitivity function. These multiple objectives on control design are met by solving the following $\mathscr{H}_\infty$ problem:

$$\arg \min_{K=[K_1 \;\; K_2]^{\mathrm{T}}} \|P\|_\infty \tag{2}$$

In practice, for the sake of computational simplicity, we relax this problem in which we seek a sub optimal controller that satisfies $\|P\|_\infty < \gamma$ for some $\gamma > \min_K \|P\|_\infty$. Note that the optimal control problem seeks a *two by one* transfer function $K = [K_1 \;\; K_2]^{\mathrm{T}}$ where K_1 decides set point regulation, resolution and control within saturation objectives while K_2 decides the extent of sample estimation error.

The problem set up presented here can be further generalized by assuming K to have a feedforward term. In the formulation presented, K has access to the deflection error signal $e = r - (y + n)$, while the formulation which includes feedforward term can separately provide the set point r and measured output $y_m := y + n$. However, in the context of the objectives discussed in this paper, the lack of feedforward controller does not create any lack of generality.

This is because this paper does not have *tracking* as an objective but instead has only *set point regulation* as an objective. However, two degrees of freedom controllers do become important when tracking becomes necessary—for instance, in Reference [21] where feedforward law operates to compensate for the sample topography by predicting the topography in advance by taking advantage of the fact that two adjacent scan lines are usually quite similar.

Remark
Note that the model in Figure 3, the noise n and the disturbance $\tilde{d}$ are indistinguishable to the estimator K_2 and therefore the problem of separating the noise and the profile is not addressed by the design of K_2. However W_d can be appropriately designed to filter out the noise.

3. A NEW SAMPLE-PROFILE SIGNAL

In this section we prescribe a profile estimate signal $\hat{d}$. The main features of this signal are (a) It gives a perfect tracking of the sample profile in the sense that the transfer function from profile $\tilde{d}$ to $\hat{d}$ is equal to one! (b) It does not create any additional complexity to the control design—in the sense that $\hat{d}$ is prescribed in terms of signals that appear when solving the $\mathscr{H}_\infty$ problem only with the first three objectives (set point regulation, high resolution and bounded control); i.e. this prescription of $\hat{d}$ renders the fourth objective of small estimation error redundant. (c) Since new estimator block does not enter the closed loop, closed loop performances remain unaffected.

The signal $\hat{d}$ is obtained by analysing the $\mathscr{H}_\infty$ feedback law designed only for the first three objectives, i.e. $\left\| \begin{array}{c} W_S S \\ W_T T \\ W_u K_1 S \end{array} \right\|$ and exploiting its quasi-observer structure. It also exploits the fact that the disturbance signal enters the plant G dynamics only in its output and not in its state evolution equation. If the state-space representations of G and the weighting functions are given by

$$G = \left[\begin{array}{c|c} A_g & B_g \\ \hline C_g & D_g \end{array}\right], \quad W_S = \left[\begin{array}{c|c} A_s & B_s \\ \hline C_s & D_s \end{array}\right], \quad W_T = \left[\begin{array}{c|c} A_t & B_t \\ \hline C_t & D_t \end{array}\right] \quad \text{and} \quad W_u = \left[\begin{array}{c|c} A_u & B_u \\ \hline C_u & D_u \end{array}\right] \tag{3}$$

then the corresponding generalized plant is described by

$$\frac{\mathrm{d}}{\mathrm{dt}} \begin{bmatrix} x_g \\ x_s \\ x_t \\ x_u \end{bmatrix} = \underbrace{\begin{bmatrix} A_g & & & \\ -B_s C_g & A_s & & \\ B_t C_y & 0 & A_t & \\ & & & A_u \end{bmatrix}}_{\triangleq A} \underbrace{\begin{bmatrix} x_g \\ x_s \\ x_t \\ x_u \end{bmatrix}}_{\triangleq x} + \underbrace{\begin{bmatrix} 0 \\ B_s \\ 0 \\ 0 \end{bmatrix}}_{\triangleq B_1} w + \underbrace{\begin{bmatrix} B_g \\ -B_s D_g \\ B_t D_g \\ B_u \end{bmatrix}}_{\triangleq B_2} u \tag{4}$$

$$\begin{bmatrix} z_1 \\ z_2 \\ z_3 \end{bmatrix} = \underbrace{\begin{bmatrix} -D_s C_g & C_s & & \\ D_T C_y & 0 & C_t & \\ & & & C_u \end{bmatrix}}_{\triangleq C_1} \begin{bmatrix} x_g \\ x_s \\ x_t \\ x_u \end{bmatrix} + \underbrace{\begin{bmatrix} D_s \\ 0 \\ 0 \end{bmatrix}}_{\triangleq D_{11}} w + \underbrace{\begin{bmatrix} -D_s D_g \\ D_t D_g \\ D_u \end{bmatrix}}_{\triangleq D_{12}} u$$

$$e = \underbrace{[-C_g \quad 0 \quad 0 \quad 0]}_{\triangleq C_2} \begin{bmatrix} x_g \\ x_s \\ x_t \\ x_u \end{bmatrix} + \underbrace{[I]}_{\triangleq D_{21}} w \underbrace{-D_g}_{\triangleq D_{22}} u,$$

where $w = r - n - \tilde{d}$ (Here we consider set point r to be 0 without any loss of generality and do not consider the effect of noise n. Its effect is considered in the next section). The $\mathscr{H}_\infty$ synthesis procedure [20, 22, 23] yields a controller K_1 which can be written as an observer-based state feedback

$$\dot{\hat{x}} = (A + B_1 F_{12\infty} + Z_\infty L_{2\infty} F_{12\infty})\hat{x} + B_2 u + Z_\infty L_{2\infty}(\underbrace{C_2\hat{x} + D_{22}\, u}_{\triangleq \hat{e}} - e) \tag{5}$$

$$u = F_{2\infty}\hat{x} \tag{6}$$

Here the matrices Z_∞, $F_{12\infty}$, $F_{2\infty}$ and $L_{2\infty}$ are described in Reference [22, pp. 451–452]. We define the estimate $\hat{d}$ of the disturbance signal $\tilde{d}$ by $\hat{d} \triangleq \hat{e} - e$, where $\hat{e} = C_2\hat{x} + D_{22}u$ is the estimate of the error, e. Therefore, if we define the state estimation error, $\tilde{x} \triangleq x - \hat{x}$ and the profile estimation error by $e_d \triangleq \hat{d} - \tilde{d}$, then

$$e_d = \hat{d} - \tilde{d} = (C_2\hat{x} + D_{22}u) - (C_2 x + D_{22}u - \tilde{d}) - \tilde{d} = -C_2\tilde{x}$$

From Equations (4) and (5), we have

$$\dot{\tilde{x}} = A\tilde{x} + B_1(w - F_{12\infty}\hat{x}) + Z_\infty L_{2\infty} F_{12\infty}\tilde{x} + Z_\infty L_{2\infty}(\tilde{d} - F_{12\infty}\hat{x})$$

$$\Rightarrow E_d(s) = -C_2\tilde{x}(s)$$

$$= -\underbrace{(C_2(sI - A - Z_\infty L_{2\infty} C_2)^{-1} B_1(w - F_{12\infty}\hat{x}))}_{\triangleq E_1(s)}$$

$$+ \underbrace{(C_2(sI - A - Z_\infty L_{2\infty} C_2)^{-1} Z_\infty L_{2\infty}(\tilde{d} - F_{12\infty}\hat{x}))}_{\triangleq E_2(s)}$$

Since, $e_d = -C_2\tilde{x}$, and $\tilde{x}$ is the state of a stable system, we expect the e_d to be small. But we prove a stronger result: that $E_1(s) = 0$ and $E_2(s) = 0$ (see Appendix A and B) by exploiting the structure of the generalized plant! This means that $E_d(s) = 0$ which implies that $\hat{d}$ tracks $\tilde{d}$ of arbitrarily large frequencies. In typical AFM designs the estimates of the sample profile, $\tilde{d}$ is obtained by processing the control signal u (as in 'constant force mode') or the deflection signal y_m (as in the 'constant height mode'). The profile estimate $\hat{d}$, on the other hand, derives information from *both* u and y_m. Note that $\hat{d}$ is prescribed only in terms of signals arising out of the design of K_1. Consequently K_2 is obtained in terms of matrices representing K_1. More precisely, by using (5), we have

$$K_1 = F_{2\infty}R \quad \text{and} \quad K_2 = -(1 + (C_2 + D_{22}F_{2\infty}))R$$

where $R \triangleq (sI - A - B_1F_{12\infty} - B_2F_{2\infty} - Z_\infty L_{2\infty}(F_{12\infty} + C_2 + D_{22}F_{2\infty}))^{-1}Z_\infty L_{2\infty}$. Also, since $E_d(s) = -(K_2S + 1)\tilde{d} = 0$, therefore $K_2S = -1$. In this context the profile estimate using $\mathscr{H}_\infty$ design does provide many advantages: (a) it is easy to design as there is plenty of commercial software that solves these optimal control problems and (b) as the signal estimate transfer function K_2 in Figure 3 comes as a consequence of design of K_1 and does not require any explicit computation—i.e. the profile estimate $\hat{d}$ is prescribed in terms of the internal signals ($\hat{e}$ and e) in the loop itself and thus does not add to the computational burden in the design procedure. Another important aspect of this design is that the class of controllers that attain the first three objectives can be parameterized as a lower linear fractional transformation (LFT) $\mathscr{F}_l(K_c, Q)$ where K_C is a *central controller* (also $K_1 = \mathscr{F}_l(K_c, 0)$) and $Q(s)$ is any stable proper transfer function such that $\|Q\|_\infty \leqslant \gamma$ where γ is performance bound as described at the end of the Section 2. Since K_2 is completely specified by K_1, this also gives a parametrization of all the controllers that satisfy all the objectives in (2).

3.1. *Robustness of this signal to plant uncertainties*

An important aspect of control design in AFM is robustness. It is especially important since the unmodelled nonlinear effects of piezoactuation such as drift and hysteresis are significant; and these devices are used in diverse operating conditions which necessitate robustness to these uncertainties. We consider a modified block diagram shown in Figure 4 to study robustness of the prescribed control design with respect to modelling uncertainties. In this model G is modified to include input and output multiplicative uncertainties. The matrix transfer function from $[r - n\ \tilde{d}]$ to the vector of regulated variables $z \triangleq [z_1\ z_2\ z_3\ z_4]^{\mathrm{T}}$ (is the same as given in (1)) describes the nominal performance. The control design prescribed in previous section ensures that the transfer functions $\|W_S S\| < 1$, $\|W_T T\| < 1$ and $\|W_u K_1 S\| < 1$. Moreover, the proposed choice of K_2 is such that $K_2S = -1$. Thus by choosing the weighting function W_d such that it is small at those frequencies where noise is significant we guarantee all the nominal performance objectives. The noise n and the disturbance $\tilde{d}$ are indistinguishable to K and therefore an appropriate filter W_d is required to separate out the two. The transfer function from perturbation inputs $\theta \triangleq [\theta_1\ \theta_2]$ to the regulated variables z describes the robust performance

$$\begin{bmatrix} z_1 \\ z_2 \\ z_3 \\ z_4 \end{bmatrix} = \begin{bmatrix} -W_S GS & -W_S S \\ W_T GS & -W_T S \\ -W_u T & W_u K_1 S \\ -W_d G K_2 S & -W_d K_2 S \end{bmatrix} \begin{bmatrix} \theta_1 \\ \theta_2 \end{bmatrix}$$

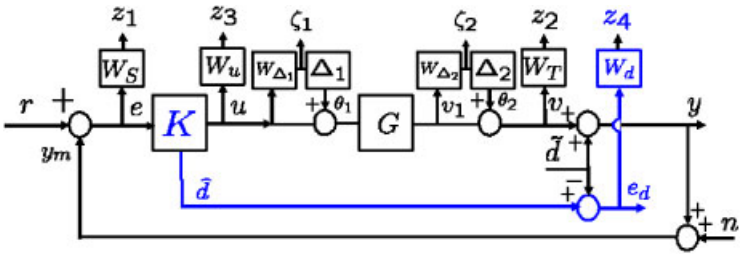

Figure 4. The schematic for the Robust $\mathscr{H}_\infty$ framework with output and input multiplicative plant uncertainties.

The control design for nominal performances for set point regulation, boundedness of control, and profile estimation error also guarantees robustness with respect to output uncertainty (with θ_2). The effect of θ_2 on z_2 given by $W_T S$ is not small but this is expected as this model fails to distinguish the output uncertainty (θ_2 which is akin to sensor noise) and the disturbance signal $\tilde{d}$. The robustness to input uncertainty (to θ_1) suggests a careful design of K to account for the trade off between nominal and robust performances. Thus designing W_S, W_T and W_d so that they shape GS, GK_1S and GK_2S instead of S, K_1S and K_2S, respectively, ensures robust performance of bandwidth, boundedness of control and profile estimation with respect to the input uncertainty. This is evident from the fact that in SISO system we can easily lump together the input and output uncertainties by transferring the input uncertainties to the output side via the plant transfer function G [20]. The transfer function from θ_2 to $[z_1 \;\; z_2]^{\mathrm{T}}$ further shows that there is a trade off between the robustness in set point regulation and high resolution with respect to input uncertainty. This trade off is captured by the fact that robust performance of both requires $W_S GS$ and $W_T GS$ to be small simultaneously. The transfer function from $[\theta_1 \;\; \theta_2]^{\mathrm{T}}$ to e_d evaluates robust performance of the proposed design. Note that since $1 + K_2S = 0$, W_d needs to be chosen so as to make W_d small at the frequencies where n and θ_2 are significant and to make W_dG small at those frequencies where θ_1 is significant. This can easily be incorporated without making any compromise on the transfer function from sample profile $\tilde{d}$ to the estimation error z_4 which remains equal to zero!

It should be emphasized that input uncertainty is not as significant as the output uncertainty as illustrated in Section 4.

4. EXPERIMENTAL SETUP AND RESULTS

The experiments were performed using MFP-3D developed by *Asylum Research Inc.*, *Santa Barbara*, *CA*. A schematic of this device is shown in Figure 5(a). XY and Z positioning stages are employed for sample positioning. A detailed description of the XY positioning stage can be found in Reference [18]. The cantilever used for the experiment is approximately 120 μm long, 5 μm width and its tip is approximately 10–20 nm in diameter. The resonant frequency of the cantilever is 13.25 kHz. The device is modified to implement the proposed control design through a software interface which was used to set up control parameters and to acquire and analyse the data (see Figure 5(b)). The cantilever deflection is sampled at 5 MHz and then filtered and down-sampled to 100 kHz. A custom code for the proposed controller (and profile estimator) which runs at 100 kHz is implemented on an ADSP-21160 Digital Signal Processor (DSP). This DSP code takes the deflection data as input and generates the control effort that is applied across the Z-piezo after amplification. The voltage range of Z-piezo is -10 to 150 V and travel range is 100 μm. The uncertainty in the input signal is mainly contributed by the Digital to Analog Converter and the uncertainty in piezo dynamics. Given 16 bit precision (Range of DAC (20 V) $\times \frac{1}{2^{16}} \times$ sensitivity (100 nm/V) $= 0.03$ nm) in DAC and small range movement reliability of piezo (sub-angstrom), output uncertainty outweighs input uncertainty. The output signal is mainly corrupted by the photo-diode noise, surface vibration and acoustic noise which add up to 0.5–0.8 nm.

System identification: The transfer function from u, the input to the Z-piezo, to the measured output y_m was obtained using frequency domain based identification techniques. Here, we chose a specific point in the operating range of the device (where its behaviour is approximately linear)

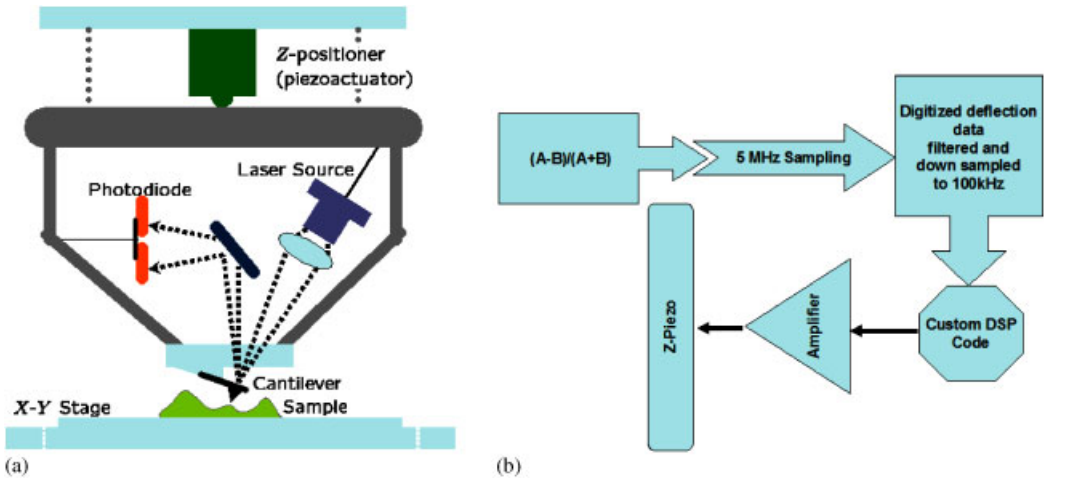

Figure 5. (a) A schematic of MFP-3D. In this device the sample is kept on a lateral scanner (X–Y positioning stage) which is a piezo actuated flexure stage. The motion in vertical direction is provided to the head which houses the cantilever and the detection system comprising of the laser and the photodiode. This motion is provided by the piezo actuated z-positioner. The photodiode output which measures the cantilever deflection is utilized by the controller K_1 to maintain the set point deflection and by K_2 to obtain the profile estimate signal; and (b) a schematic of the controller-estimator implementation.

and obtained a model of the device at this point by studying its frequency response over a pre-specified bandwidth. The frequency response of the device at this operating point over a 2 kHz bandwidth is shown in the bode plot (dashed lines) in Figure 6. Accordingly, an eleventh-order stable transfer function

$$G = \times \frac{-8.208 \times 10^3 (s^2 + 530.9s + 3.132 \times 10^7)(s^2 + 472s + 1.558 \times 10^8)(s^2 + 868.3s + 2.734 \times 10^8)}{(s + 2.513 \times 10^4)(s^2 + 768s + 3.146 \times 10^7)(s^2 + 615.8s + 1.422 \times 10^8)(s^2 + 918.9s + 1.777 \times 10^8)}$$
$$\times \frac{(s^2 + 249.1s + 3.011 \times 10^8)(s^2 - 2.827 \times 10^4 s + 5.021 \times 10^8)}{(s^2 + 508.8s + 2.789 \times 10^8)(s^2 + 377.1s + 3.056 \times 10^8)}$$

was fit to this data. Figure 6 shows that there is a good match between this frequency response data and the one fitted to the data, $G(s)$.

Control design, implementation and validation: The control transfer function K_1 was obtained using the hinf function in MATLAB. In this design, the weighting function W_S is chosen such that it has high gains at low frequencies and low gains at high frequencies (see Figure 7(a)). This scaling ensures that the optimal feedback law is such that the sensitivity function is small at low frequencies, thus guaranteeing good set point regulation at the concerned frequencies. More precisely, W_S was chosen to be a first-order transfer function, $W_s(s) = (0.3333s + 2199)/(s + 2.199)$. This transfer function is designed so that its inverse (an approximate upper bound on the sensitivity function) has a gain of -60 dB at low frequencies (less than 100 Hz) and a gain of ≈ 9.5 dB above 1000 Hz. The weight W_T was chosen to be $W_T(S) = (s + 2199)/(10^{-5}s + 1.1 \times 10^4)$ which has high gains (100 dB) at high frequencies (note that noise is in the high frequency region) to ensure high resolution. The transfer function, $K_1 S$ was scaled by a

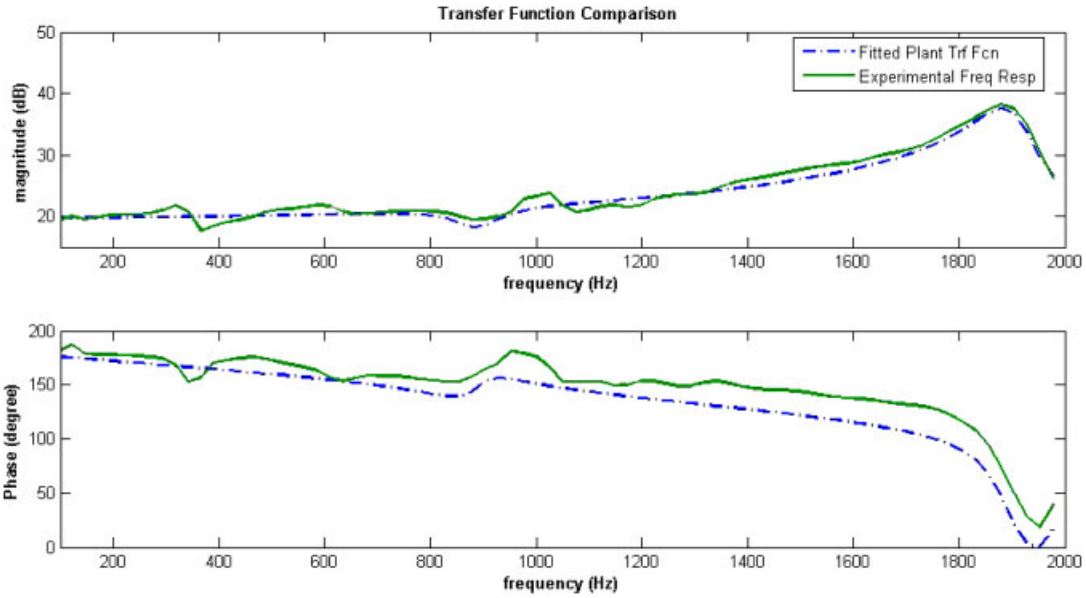

Figure 6. Experimentally (solid) obtained frequency response is compared with that of the model (dotted) G.

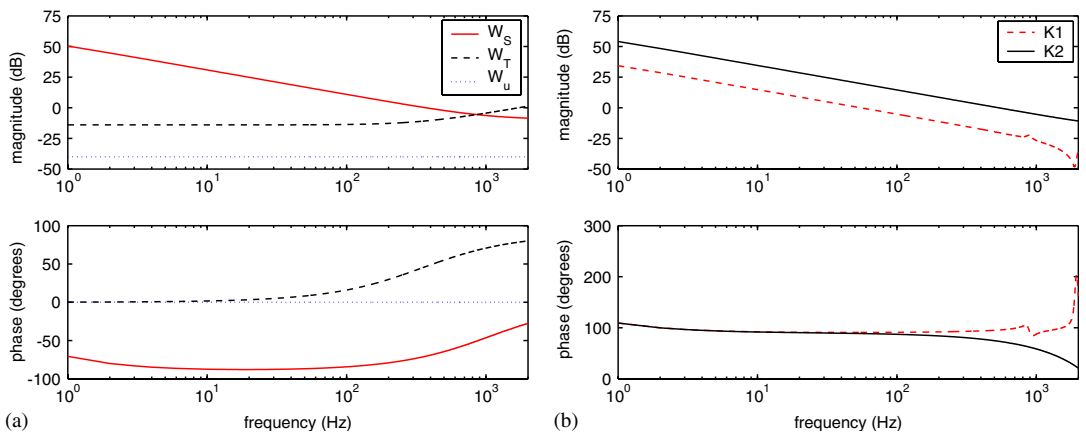

Figure 7. Control Design: (a) Weighting functions for Sensitivity, Complementary Sensitivity and Actuation signal (W_S, W_T and W_u), respectively; and (b) transfer functions of controller K_1 and observer K_2 obtained from hinfsyn design.

constant weighting $W_u = 40$ dB, to restrict the magnitude of the input signals such that they are within the saturation limits. This weighting constant gives control signals that are at most six times the reference signals.

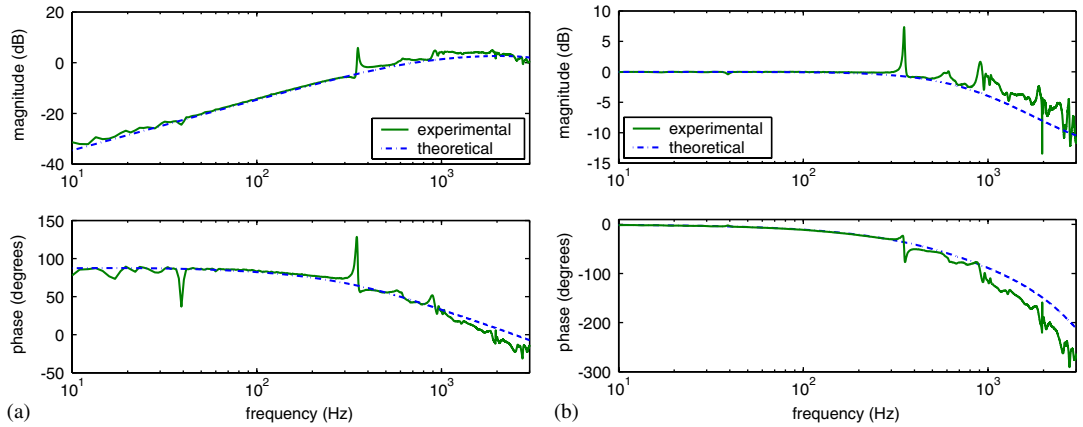

Figure 8. Experimental validation: (a) and (b) The plot compares the simulated and the experimentally obtained sensitivity and complementary transfer functions, respectively. There is a good match between the two.

The $\mathscr{H}_\infty$ design resulted in transfer functions for K_1 and K_2 (the transfer functions are given in Appendix A and B). Figure 7(b) shows the controller and observer obtained from the solution of stacked $\mathscr{H}_\infty$ problem. Note that K_1 and K_2 have a similar dynamics at low frequencies and therefore give similar images at these frequencies. These transfer functions were implemented on the DSP and the signals $\hat{d}, r$, and u were recorded and used to evaluate images. The implementation of the loop was validated by comparing the closed loop transfer functions obtained using HP-Signal analyser with the simulated ones. Figure 8 shows experimental and theoretical frequency response of sensitivity and complementary sensitivity functions. As seen in the figures, experimental and theoretical responses match closely except at a particular frequency range around 400 Hz.

Results: To study the performance of the new estimate signal, it was compared to and contrasted with the typically used control signal. Figure 9(a) shows that the bandwidth of the transfer function T_{ud} has a bandwidth of approximately 800 Hz whereas the magnitude of $T_{\hat{d}d}$ (in Figure 9(b)) is within 3 dB for the whole range considered. The phase plots show considerable phase drop for the T_{ud} while near zero phase for the $T_{\hat{d}d}$. This explains the difference seen in the trace and the retrace scans when using the u signal for the image. It is important to note that the bandwidth of 800 Hz for the transfer function T_{ud} is by itself a huge improvement over typical commercial AFMs (which have imaging bandwidth in order of few tens of Hertz).

It is shown analytically that $T_{\hat{d}d}$ is identically equal to one—however, the experimental transfer function $T_{\hat{d}d}$ slightly deviates from one (see Figure 9). The reason, after careful analysis and experiments, was attributed to the fact that there is an uncertain pole-zero pair (near 400 Hz) in the plant G. On repeating the experiments to obtain the frequency response of G showed that the location of the pole-zero pair is not constant. Since the design presented here is model-based, this uncertainty leads to minor mismatch between the simulations and the experiments. There are other regions in the frequency range where there is a mismatch (though within 3 dB) between sample profile and its estimate. This is again attributed to the inherent

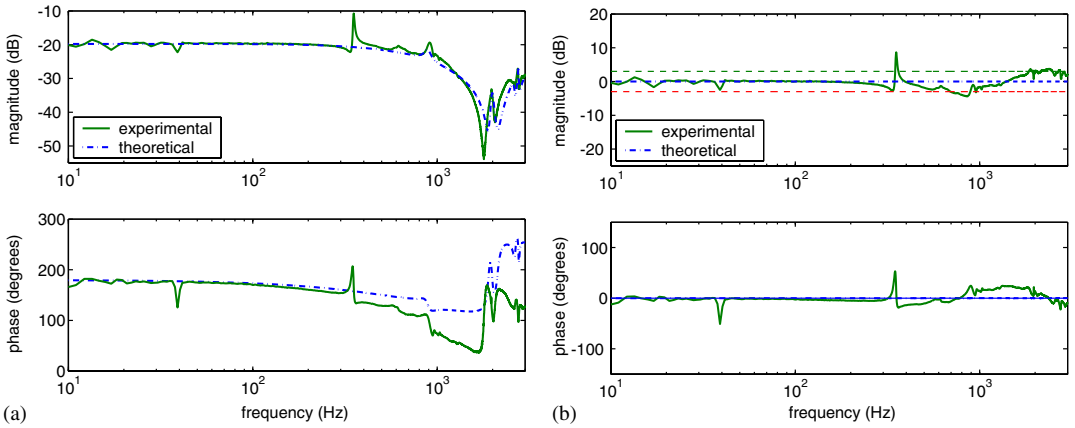

Figure 9. (a) The experimental frequency response of the control effort u to sample topography showing that it is not a good estimate of topography at high frequencies. (b) The experimental frequency response of the estimate $\hat{d}$ to sample topography remains flat corroborating the analytical result that this transfer function is a constant, the magnitude plot is within ± 3 dB and the phase is near zero over the entire range.

constraint of model based designs. Due to limited computation power, it is not possible (and also not advisable) to fit an arbitrary higher order plant to the physical system. However, the sensitivity to this mismatch is incorporated in the design procedure by appropriately shaping the K_2S transfer function.

In addition to investigating the above transfer functions, imaging experiments were performed to test the proposed profile estimate signal. A gold calibration grid with squares of height 180 nm every 10 μm was used for imaging using the $\hat{d}$ signal. This image was compared with the one obtained from the control signal u. In the first experiment, the grating was scanned at 10 Hz and the corresponding control signal u and the proposed estimate signal $\hat{d}$ were recorded. The control signal was proportional to the profile, in fact $u \approx -0.1d$. Therefore, u signal was magnified by ≈ 10 times to get the profile estimate. The resulting data is shown in Figure 10(a). Note that the scanned image with the proposed signal is superior to the image with the u signal. This is more evident in the plots showing a particular line scan, where the image with u has an oscillatory behaviour in response to the higher frequency content of the square profile. The main feature of the proposed signal is the high bandwidth it achieves. The difference in performance between the $\hat{d}$ and u signals is much greater in faster scans. This is shown in Figure 10(b). Here the scan was done at 150, 500 and 1400 Hz where the reference signal was generated on the computer itself and downloaded onto the DSP card to mimic a sinusoidal sample profile. At low frequencies (below the bandwidth of T_{ud}) the control signal u is a good measure of d. However, there is a significant phase lag between the d and the u signal at 500 Hz. At higher frequency (1400 Hz) control signal gives a poor estimate of d—it is attenuated (by more than 50%) and has considerable phase lag. The experimental results show that the proposed signal $\hat{d}$ tracks near perfectly the reference signal even at these high bandwidths, as well as in lower frequencies. This fact is corroborated from the frequency response of transfer functions shown in Figure 9, where T_{ud} rolls off

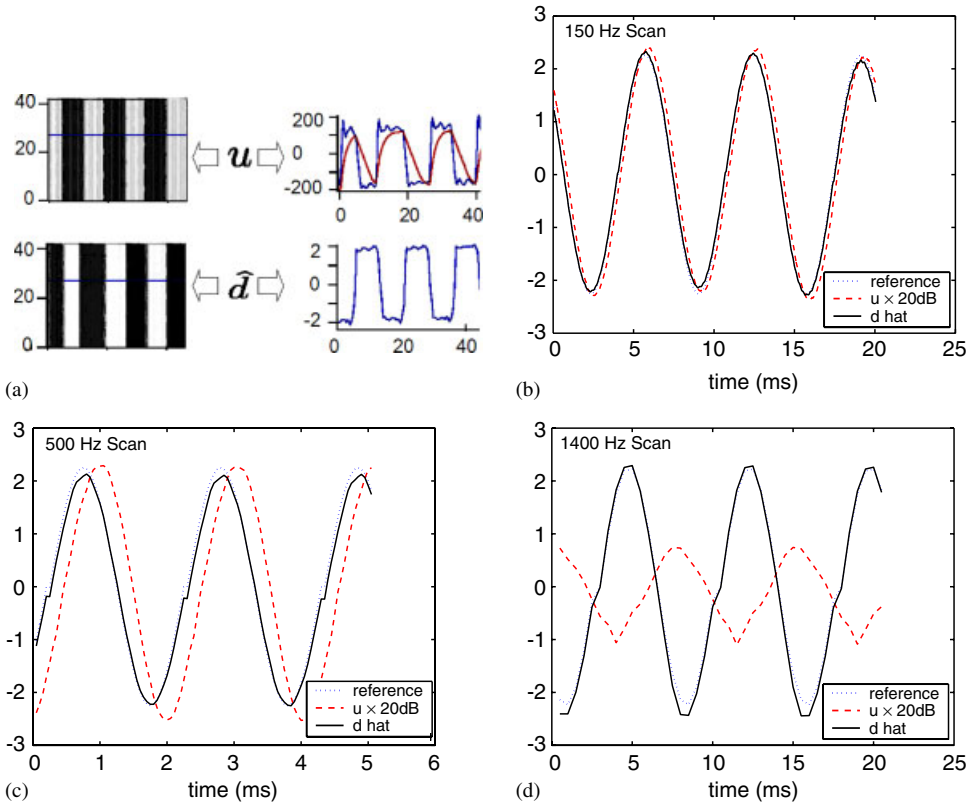

Figure 10. (a) Experimental data showing significantly superior images (left panel) obtained by using the new imaging signal $\hat{d}$ compared to the use of the control effort u as the sample topography estimate; (b,c) the u signal gives worse estimates as the frequency of the d is increased (150 and 500 Hz). The magnitude plots are consistent but there is a considerable phase lag. The $\hat{d}$ signal on the other hand, has practically no phase lag; and (d) experimental data that shows that the new imaging signal $\hat{d}$ follows a 1.4 kHz reference sine wave that the control signal is unable to track at all.

after 800 Hz with significant phase lag but $T_{\hat{d}d}$ remains with ± 3 dB with almost zero phase. This imaging at 1.4 kHz demonstrates a substantial improvement over the existing technology where images are usually scanned at few tens of Hertz. This same algorithm was also implemented on another AFM (Veeco Instruments, Santa Barbara, CA) and experimental results again corroborated that $T_{\hat{d}d} \approx 1$ (results not shown here).

5. CONCLUSIONS

The imaging problem in an Atomic Force Microscope is addressed using modern control theory. An optimal control problem is formulated to address the design of a new profile estimate signal which is valid even for fast scanning in Atomic Force Microscopy. The objectives of set

point regulation and high resolution are also included in the formulation. The solution of this problem yields a new estimate of the sample profile, $\hat{d}$ and it is *proved* that the transfer function from the profile to the estimate is 1. The design was implemented and a substantial improvement over traditional designs is shown. Typical controllers in commercial AFMs use PID feedback laws which do not give reliable images beyond a few tens of Hertz bandwidth while experiments with the proposed signal at 1400 Hz gave faithful images. Experiments show a significant improvement in bandwidth in sample-profile estimation. The proposed signal makes use of *both* the control signal u and the deflection error signal e smartly to give the sample profile in contrast to using only the control signal u in constant force imaging and using only the deflection error signal e in constant height imaging.

Advanced control tools have been used to tackle an important problem in atomic force microscopy. This work further demonstrates the immense scope for control theoretic tools to improve the bandwidth, resolution and reliability of these devices.

APPENDIX A: TO SHOW THAT $E_1(s) = 0$ AND $E_2(s) = 0$

This derivation relies on the structure of the generalized plant P and the quasi-observer form of the $\mathscr{H}_\infty$ controller developed in Reference [22, pp. 451–452]. The transfer function, G is proper which implies that $D_{22} = D_g = 0$. This coupled with structure of P, when substituted in equations give $Z_\infty = I$ and $L_{2\infty}$ is product of B_1 and another matrix, i.e. $Z_\infty L_{2\infty}$ is of the form $B_1 \times$. This implies that both E_1 and E_2 are of the form $C_2(sI - A - Z_\infty L_{2\infty} C_2)^{-1} B_1 \times$ and therefore it is enough to show that $C_2(sI - A - Z_\infty L_{2\infty} C_2)^{-1} B_1 = 0$.

By using the fact that A is stable and the identity $(I - uv')^{-1} = (I + uv'/(1 - v'u))$ for column vectors u and v, we show that

$$
\begin{aligned}
C_2(sI - A - Z_\infty L_{2\infty} C_2)^{-1} B_1 &= C_2(sI - A)^{-1} \left(I - \underbrace{Z_\infty L_{2\infty}}_{u} \; \underbrace{C_2(sI - A)^{-1}}_{v'} \right)^{-1} B_1 \\
&= C_2(sI - A)^{-1} \left(I + \frac{Z_\infty L_{2\infty} C_2(sI - A)^{-1}}{1 - C_2(sI - A)^{-1} Z_\infty L_{2\infty}} \right) B_1 \\
&= \frac{C_2(sI - A)^{-1} B_1}{1 - C_2(sI - A)^{-1} Z_\infty L_{2\infty}} \qquad \text{(A1)}
\end{aligned}
$$

This in turn implies that it is enough to show that $C_2 = (sI - A)^{-1} B_1 = 0$. Now $C_2[-C_g \; 0]$ and A is of lower block triangular form $A = \begin{bmatrix} A_g & 0 \\ \times & \times \end{bmatrix}$ and B_1 is of the form $\begin{bmatrix} 0 \\ \times \end{bmatrix}$. After noting that $(sI - A)^{-1}$ is itself a lower block triangular matrix

$$
C_2(sI - A)^{-1} B_1 = \begin{bmatrix} -C_g & 0 \end{bmatrix} \begin{bmatrix} (sI - A_g)^{-1} & 0 \\ \times & \times \end{bmatrix} \begin{bmatrix} 0 \\ \times \end{bmatrix} = 0
$$

Hence $E_1(s) = 0$ and $E_2(s) = 0$.

APPENDIX B: THE CONTROLLER $[K_1 \ K_2]^T$ FROM THE $\mathscr{H}_\infty$ DESIGN

The $\mathscr{H}_\infty$ design resulted in controllers K_1 and K_2 given by

$$K_1 = (-6.4657 \times 10^{-10}) \times \frac{(s+2.364\times10^{17})(s+1.1\times10^{9})(s+2.513\times10^{4})(s^2+768s+3.146\times10^{7})(s^2+615.8s+1.422\times10^{8})}{(s+2.567\times10^{6})(s+2.199)(s+8.208\times10^{11})(s^2+530.9s+3.132\times10^{7})(s^2+472s+1.558\times10^{8})} \times \frac{(s^2+918.9s+1.777\times10^{8})(s^2+508.8s+2.789\times10^{8})(s^2+377.1s+3.056\times10^{8})}{(s^2+868.3s+2.734\times10^{8})(s^2+249.1s+3.011\times10^{8})(s^2+2.733\times10^{4}s+9.793\times10^{8})}$$

$$K_2 = (9.2684 \times 10^{-16}) \times \frac{(s+1.1\times10^{9})(s+1.163\times10^{14})(s-1.164\times10^{14})(s^2+530.9s+3.132\times10^{7})}{(s+2.567\times10^{6})(s+2.199)(s+8.208\times10^{11})(s^2+530.9s+3.132\times10^{7})(s^2+472s+1.558\times10^{8})} \times \frac{(s^2+472s+1.558\times10^{8})(s^2+868.3s+2.734\times10^{8})(s^2+249.1s+3.011\times10^{8})(s^2-2.827\times10^{4}s+5.021\times10^{8})}{(s^2+868.3s+2.734\times10^{8})(s^2+249.1s+3.011\times10^{8})(s^2+2.733\times10^{4}s+9.793\times10^{8})}$$

ACKNOWLEDGEMENTS

We would like to acknowledge the constant support of Dr Jason Cleveland and Dr Anil Gannepalli of *Asylum Research* and thank them for all the help during the course of the project. We also acknowledge NSF for this work was supported by NSF grants ECS 0449310 CAR to Prof. Srinivasa M. Salapaka from University of Illinois, and CMS 0301516 and CMS 0201560 to Prof. Murti V. Salapaka from Nano Dynamics Laboratory at Iowa State University.

REFERENCES

1. Binnig G, Quate CF, Gerber C. Atomic force microscopy. *Physics Review Letters* 1986; **56**:930–933.
2. Bhushan B. *Handbook of Micro/Nano Tribology*. CRC Press: Boca Raton, FL, 1995.
3. Bonnel D. *Scanning Probe Microscopy and Spectroscopy*: *Theory*, *Techniques and Applications* (2nd edn). Wiley: New York, 2000.
4. Israelachvili J. *Intermolecular and Surface Forces* (2nd edn). Academic Press, Harcourt Brace & Company: New York, 1991.
5. Sebastian A, Salapaka MV, Chen DJ, Cleveland JP. Harmonic and power balance tools for tapping-mode AFM. *Journal of Applied Physics* 2001; **89**(11):6473–6480.
6. Lee S-I, Howell S, Raman A, Reifenberger R. Nonlinear dynamics of microcantilevers in tapping mode atomic force microscopy—comparison between theory and experiment. *Physical Review B* 2002; **66**(11):1–10.
7. Ashhab M. Salapaka MV, Dahleh M, Mezic I. Dynamical analysis and control of micro-cantilevers. *Automatica* 1999; **35**(10):1663–1670.
8. Salapaka S, Dahleh M, Mezic I. On the dynamics of a harmonic oscillator undergoing impacts with a vibrating platform. *Nonlinear Dynamics* 2001; **24**:333–358.
9. Sebastian A, Gannepalli A, Salapaka MV. The amplitude phase dynamics and fixed points in tapping-mode atomic force microscopy. In *Proceedings of the American Control Conference*, Boston, July 2004; 2499–2504.
10. Salapaka MV, Bergh HS, Lai J, Majumdar A, McFarland E. Multimode noise analysis of cantilevers for scanning probe microscopy. *Journal of Applied Physics* 1997; **81**(6):2480–2487.
11. Sahoo DR, Sebastian A, Salapaka MV. Transient-signal-based sample-detection in atomic force microscopy. *Applied Physics Letters* 2003; **83**(26):5521–5523.
12. Napoli M, Bamieh B, Dahleh M. Optimal control of arrays of microcantilevers. *Journal of Dynamic Systems Measurement and Control* 1999; **121**:686–690.
13. Napoli M, Bamieh B, Turner K. Mathematical modeling, experimental validation and observer design for a capacitively actuated microcantilever. *Proceedings of the American Control Conference*, Denver, CO, 4–6 June 2003.

14. Daniele A, Salapaka S, Salapaka MV, Dahleh M. Piezoelectric scanners for atomic force microscopes: design of lateral sensors, identification and control. In *Proceedings of the American Control Conference*, San Diego, CA, June 1999; 253–257.
15. Schitter G, Menold P, Knapp HF, Allgower F, Stemmer A. High performance feedback for fast scanning atomic force microscopes. *Review of Scientific Instruments* 2001; **72**(8):3320–3327.
16. Croft D, Shedd G, Devasia S. Creep, hysteresis and vibration compensation for piezoactuators: atomic force microscopy application. *Journal of Dynamic Systems, Measurement and Control* 2001; **123**:35–43.
17. Salapaka S, Sebastian A, Cleveland JP, Salapaka MV. High bandwidth nano-positioner: a robust control approach. *Review of Scientific Instruments* 2002; **73**(9):3232–3241.
18. Sebastian A, Salapaka S. $\mathscr{H}_\infty$ loop shaping design for nano-positioning. In *Proceedings of the American Control Conference*, Denver, CO, June 2003; 3708–3713.
19. Sebastian A, Cleveland JP, Salapaka MV. Robust control approach to atomic force microscopy. In *Proceedings of the IEEE Conference on Decision and Control*, Hawai, December 2003; 3443–3444.
20. Skogestad S, Postlethwaite I. *Multivariable Feedback Control, Analysis and Design*. Wiley: New York, 1997.
21. Schitter G, Allgower F, Stemmer A. A new control strategy for high speed atomic force microscopy. *Nanotechnology* 2004; **15**(1):108–114.
22. Zhou K, Doyle JC, Glover K. *Robust and Optimal Control*. Prentice-Hall: Upper Saddle River, NJ, 1996.
23. Doyle JC, Glover K, Khargonekar PP, Francis BA. State-space solutions to standard $\mathscr{H}_2$ and $\mathscr{H}_\infty$ control problems. *IEEE Transactions on Automatic Control* 1989; **34**(8):831–847.

